Tellus (1989), *41B*, 32–50

Ionic concentrations and initial S(IV)-oxidation rates in droplets during the condensational stage of cloud

By WINFRIED SEIDL, *Meteorologisches Institut der Universität München, Theresienstraße 37, D-8000 München 2, FRG*

(Manuscript received 12 January 1988; in final form 12 July 1988)

ABSTRACT

Concentrations of ions and the catalytic active trace metals iron and manganese, pH-values and S(IV)-oxidation rates are calculated in cloud droplets of different size in the beginning stage of a cloud. The calculations are based on size-dependent chemical composition of mixed-aerosol particles. The condensation process is modeled by using an adiabatic parcel model. High concentrations of all ions and metals are found in the interstitial particles. Sulfate, nitrate and ammonium have concentrations in the range $1.4 \cdot 10^{-2}$ to 2.4 moles/l. The pH-values are generally between 1.3 and 1.7. In the small, activated cloud droplets of approximately 5 μm radius, ions and metals have the smallest concentrations in the order of 10^{-6} to 10^{-4} moles/l for the ions and 10^{-8} to 10^{-7} moles/l for Mn and Fe. Higher concentrations up to $7.5 \cdot 10^{-2}$ moles/l are found in the larger, growing droplets for the ions as well as for the metals. These concentrations are used to calculate the initial oxidation rates of sulfur(IV) to sulfur(VI) in the presence of hydrogen peroxide, ozone and the catalytic active metals Fe and Mn. Depending on the initial pH-value the oxidation rates can differ considerably in different sized cloud droplets. Regarding the whole parcel, the largest fraction of sulfate is produced in the large liquid water volume of the cloud droplets. In the interstitial particles, only a negligible fraction is produced. Basic droplets can increase the initial production rate of S(VI) considerably, but small droplets will become acidic after a few seconds by the given pressures of O_3 and SO_2. The oxidation rates in large, basic droplets would also be high, but they are limited by gas-phase diffusion of the reagents to the droplets. The initial oxidation rate of S(IV) calculated from summing the rates of the individual droplet classes is higher than the rate calculated for bulk cloud water with mean chemical composition.

1. Introduction

The development of cloud droplets on aerosol particles has been modeled in a number of studies for approximately the past 30 years. By comparison with measurements (e.g., Diem, 1948), Mordy (1959) already found that an adiabatic parcel model is suitable for description of the number concentration and the size of cloud droplets near the cloud base. These models show that most of the water condenses on the small activated cloud droplets with radii of 4 to 5 μm which originate from aerosol particles with dry volume equivalent radii between 0.04 and 0.2 μm (sizes given in this section are for an updraft velocity of 1 m/s and a rural aerosol type). The smaller particles are not activated in the cloud and form the interstitial aerosol with radii smaller than 0.4 μm. The growth rate of the largest aerosol particles is limited by the diffusion of water vapor to their surface. They need a longer time to reach their critical radii, as they are not in the region of unstable growth (Fig. 1). Thus, particles with dry volume equivalent radii larger than approximately 0.2 μm are not activated near the cloud base (Jensen and Charleson, 1984; Hänel, 1987). However, in this paper, they will be called "large droplets" for three reasons: they are growing in the cloud; their radii are larger than the radii of the activated droplets; their size

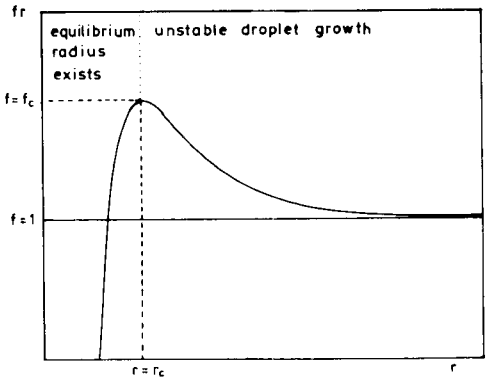

Fig. 1. Relative humidity f_r above the surface of the droplet. The critical radius r_c and the critical relative humidity f_c are marked. For $r > r_c$, no equilibrium radius exists for a given relative humidity: the droplet is activated and grows unstable.

is large enough that they can be scavenged by falling precipitation particles (Jensen and Charlson, 1984). The largest droplets have radii of approximately 30 μm even near the cloud base. They can grow further by coalescence (Pruppacher and Klett, 1978).

Measurements of the chemical composition of the aerosol particles have shown a different composition for fine particles (smaller than approximately 2.5 μm diameter) and for coarse particles (larger than 2.5 μm diameter). The fine particles are mainly composed of sulfate, nitrate, and ammonium and are usually acidic (Brosset, 1976; Harrison and Pio, 1981). The larger coarse-mode particles mainly consist of mineral dust or sea salt and sometimes they are basic. The largest mass fractions of iron and manganese are usually found in the coarse mode, but the fine particles also contain these metals (Milford and Davidson, 1985).

The oxidation rates of sulfur(IV) by ozone and by oxygen catalyzed by iron and manganese depend on the pH-value of the aqueous solution and on the concentrations of the metals (Hoffmann and Calvert, 1985). Therefore, different oxidation rates in droplets of different sizes are expected, dependent on the pH-values and the concentrations of the catalytic active metals.

Previous studies of this oxidation process do not consider the aerosol properties in detail. Tremblay and Leighton (1986), Walceck and Taylor (1986) and Hough (1987) model the cloud water as a bulk phase. They found pH-values in the range of approximately 3.0 to 5.5. In this range of pH-values, H_2O_2 makes a large contribution to the sulfate production, except when daytime photochemical reactions produce a considerable amount of the radicals HO_2 and OH (Hough, 1987). Lee (1986) considers cloud droplets of different size on a basis of a simplified aerosol composition. The droplets have pH-values in the range between less than 2 and 5.3. He also found a large influence of H_2O_2.

In this study, the model calculations are based on mixed aerosol particles to get droplet pH-values and metal concentrations as realistic as possible. The chemical compositions of the aerosol types used are derived from measurements. The initial stage of the cloud is especially investigated, in which the chemical composition of the cloud droplets is influenced by the composition of the aerosol particles which have acted as cloud nuclei. The concentrations of ions and catalytic active metals in different sized droplets can be used directly as input data for cloud models with more complex microphysics and dynamics.

2. Methods

An adiabatic parcel model (Hänel, 1987) is used. A parcel of air containing 60 size classes of aerosol particles with dry volume equivalent radii between 0.01 and 10 μm is transported upward with a constant velocity w. The model calculations are started at 60% relative humidity. A linearized version of the droplet growth equation is used, which can be integrated analytically (Hänel, 1987). Particles with small thermodynamic relaxation times are in equilibrium with the ambient relative humidity. For these particles, the equilibrium radii were calculated. The calculation of their radii by integrating the droplet growth equation would require very small time steps for numerical stability. By using the equilibrium condition, these problems can be avoided.

The relative humidity f_r at the surface of a droplet or particle with radius r and dry volume equivalent radius r_o is described by the following equation:

$$f_r = \exp\left(\frac{A^\circ}{r} - \frac{B^\circ}{(r/r_o)^3 - 1}\right). \quad (1)$$

Eq. (1) is necessary for calculation of the condensation growth by the droplet growth equation (see Appendix), and for calculation of the equilibrium radius of an aerosol particle. The equation contains two simplifications: The curvature parameter A° and the activation parameter B° are defined for infinite dilution of the electrolyte solution. The use of these parameters is possible, because cloud droplets and aerosol particles at relative humidities near 100% consist of diluted electrolyte solutions. With these parameters, a fast evaluation of the equilibrium radius and an analytical integration of the droplet growth equation are possible. However, the size of an aerosol particle at smaller relative humidities is described schematically, and in particular, a hysteresis effect (Hänel, 1976) cannot be described.

The curvature parameter for infinite dilution A° contains the surface tension of a pure water droplet:

$$A^\circ = \frac{2 \cdot \sigma_w}{\rho_w \cdot R_w \cdot T}, \tag{2}$$

with σ_w the surface tension, ρ_w the density of pure water and R_w the specific gas constant of water vapor.

The activation parameter B° describes the hygroscopicity of the droplet for infinite dilution of the electrolyte solution. Measurements of the activation parameter are difficult and are therefore rare. Hänel (1976) and Hänel and Lehmann (1981) measured the growth of aerosol particles with increasing relative humidity and determined the activation parameter by extrapolation of their data to infinite dilution. Hoppel (1979) and Fitzgerald et al. (1982) used another method: They segregated the aerosol particles by size using a diffusion battery and measured the supersaturation necessary to activate them in a cloud condensation chamber. From the known size and supersaturation of the particles, the activation parameter can be calculated.

The information about the activation parameter obtained by these authors is not sufficient for use as input data for this study for two reasons. First, there are very few size-segregated measurements. Hänel and Lehmann (1981) performed two measurements on samples from Deuselbach, a rural location in Germany, and Fitzgerald et al. (1982) segregated the aerosol into 3 size categories, but all smaller than 0.1 μm. Secondly, there is no direct relation to the chemical composition of the aerosol particle, especially to the concentrations of H^+ or OH^- and to the catalytic active metals iron and manganese.

Therefore, the activation parameter is evaluated from the chemical composition of the particles. For this, it is assumed that the particles in a specific size range are mixed particles all of the same composition of different electrolytes and insoluble material. The activation parameter can be written in the following way:

$$B^\circ = \frac{\rho_o \cdot M_w \cdot m_s}{\rho_w \cdot M_s \cdot m_o}, \tag{3}$$

with M_s the mean molar mass of the ions i (Thudium, 1978):

$$M_s = \frac{\sum_i m_i}{\sum_i m_i / M_i}. \tag{4}$$

This description was chosen because the ions are usually determined by chemical analysis of aerosol samples, taken by multistage impactors. Here, ρ_o is the mean density of the dry particulate material and ρ_w the density of the pure water. M_w is the molar mass of the water, m_s the mass of the water-soluble material of the particles, m_o the total dry mass of the particles, m_i the mass and M_i the molar mass of the ion i.

The mean bulk density of the dry particulate material can be calculated according to Hänel (1976):

$$\rho_o = \frac{\sum_k m_k}{\sum_k m_k / \rho_{ok}}. \tag{5}$$

For the soluble fraction, the density cannot be determined from the concentrations of the ions directly; they had to be "combined" with substances beforehand. The positive ions were distributed among the negative ions according to the relative frequency of the negative charges:

$$n_{ij} = \frac{n_i^+ \cdot n_j^- \cdot z_j^-}{\nu_{ij} \cdot \sum_j n_j^- \cdot z_j^-}, \tag{6}$$

with n the mole number and z the number of elementary charges of the positive ions i and the negative ions j. n_{ij} is the mole number of the substance ij and ν_{ij} is the number of the positive

ions per molecule of the substance *ij*. This simple apportionment is possible because the mean density does not depend strongly on the distribution of the ions to substances. Table 1 shows, e.g., that the sulfates always have a higher density than the chlorides, and that the ratio is nearly the same. Therefore, different apportionments of the ions to substances based on the same ionic concentrations result approximately in the same mean density. This was tested for some ionic compositions typical for atmospheric aerosol by preferring one time substances with high densities and the other time substances with low densities. The differences of the mean densities were not larger than $\pm 3\%$.

This simple apportionment of the ions to electrolytes should be used only for determination of the mean bulk density, because the apportionment is different from the real one. The electrolytes are, however, dissolved in aerosol particles at high relative humidities and in cloud droplets, so that an apportionment of the ions to the real electrolytes is not necessary. (However, even by this simple apportionment, for the given ionic concentrations, e.g., for the fine particles, the largest mass fraction of the water-soluble material consists of the electrolytes $(NH_4)_2SO_4$, H_2SO_4, NH_4NO_3, ..., which are commonly observed in the atmosphere.)

Table 1. *Dry densities of electrolytes*

	Densities (g/cm³)				
	NO_3^-	Cl^-	SO_4^{2-}	Br^-	OH^-
H^+	HNO_3		H_2SO_4		
	1.503		1.841		
NH_4^+	NH_4NO_3	NH_4Cl	$(NH_4)_2SO_4$	NH_4Br	
	1.725	1.527	1.769	2.429	
Na^+	$NaNO_3$	NaCl	Na_2SO_4	NaBr	NaOH
	2.261	2.165	2.680	3.203	2.130
K^+	KNO_3	KCl	K_2SO_4	KBr	KOH
	2.109	1.984	2.662	2.750	2.044
Ca^{2+}	$Ca(NO_3)_2$	$CaCl_2$	$CaSO_4$	$CaBr_2$	$Ca(OH)_2$
	2.504	2.150	2.960	3.353	2.240
Mg^{2+}		$MgCl_2$	$MgSO_4$	$MgBr_2$	$Mg(OH)_2$
		2.320	2.660	3.720	2.360
Al^{3+}		$AlCl_3$	$Al_2(SO_4)_3$	$AlBr_3$	$Al(OH)_3$
		2.440	2.710	2.640	2.420
Fe^{3+}		$FeCl_3$	$Fe_2(SO_4)_3$		
		2.898	3.097		
Pb^{2+}	$Pb(NO_3)_2$	$PbCl_2$	$PbSO_4$	$PbBr_2$	
	4.530	5.850	6.200	6.660	
Zn^{2+}			$ZnSO_4$		
			3.540		
Mn^{2+}			$MnSO_4$		
			3.250		
Cu^{2+}			$CuSO_4$		
			3.603		
Cr^{3+}			$Cr_2(SO_4)_3$		
			3.012		

3. Input data sets

To get reliable results on the concentration of ions and catalytic active metals in droplets, complete data sets of the size-dependent chemical composition of the aerosol particles have to be chosen as input data. In the literature, no single data set suitable for this has been found. Therefore, two types of aerosol composition have been created based on suitable measurements.

For Case A, two sets of measured aerosol composition have been fitted, one containing ionic concentrations (Schumann et al., 1986), the other elemental concentrations. For a background location in Switzerland, Schumann et al. (1986) measured the ionic composition of an aerosol sample taken by a multistage impactor. They analyzed the ions NH_4^+, SO_4^{2-}, NO_3^-, Cl^-, Na^+, K^+, Mg^{2+}, Ca^{2+}. In general, the highest mass fraction of the water-soluble mass of a rural aerosol consist of these ions. Thus, the concentrations of H^+ or OH^- can be derived reliably from electroneutrality. This data set contains no information on the insoluble mass fraction and the catalytic active metals. Therefore, a data set of elemental concentrations with a similar size distribution of sulfur measured at a sample from the Wetterau, a rural location in Germany (Richter and Wätjen, 1980) was fitted. Additionally, the assumption was made that 50% of the fine-particle mass is water-insoluble carbonaceous material. This was done because measurements at rural locations in the USA showed a similar feature (e.g., Reible et al., 1982).

A second data set (Case B) used for this study was also measured at an aerosol sample from a rural location in Germany. Höfken et al. (1981) analyzed concentrations of ions and metals of an aerosol probe sampled by a multistage impactor at Solling, a forested location in Germany. This

data set is suitable for this study because the ions sulfate, ammonium, nitrate and chloride, are analyzed together with the concentrations of the catalytic active metals iron and manganese. For the fine particles, the analyzed ions normally have the largest mass fractions of the water-soluble material, so the concentration of H^+ can be calculated reliably from the condition of electroneutrality. Unfortunately, the metal ions Na^+, K^+, Mg^{2+} and Ca^{2+}, which normally have high mass fractions of the water-soluble material in the coarse particle mode, were not measured. To evaluate the H^+ concentration from electroneutrality, assumptions about the concentrations of these metal ions had to be made. The concentrations of the elements were calculated from their mean ratio to iron in the earth's crust. This method has to be regarded as a rough estimation only. It neglects the fact that ions can also originate from other natural sources like sea salt or anthropogenic sources like road dust or fly ash. However, the atmospheric life-times of coarse-mode particles are short, and therefore they mainly originate from local sources. The measurement site was located in a continental, forested area. Therefore, contributions from sea salt or anthropogenic sources are not likely. However, they cannot be excluded.

No additional fraction of carbonaceous material has been assumed in this case. Therefore, the water-soluble mass fraction is larger in this case than in Case A, resulting in a higher B^o. Through this the influence of different mass fractions of water-soluble material can be tested. The soluble part of the metals was obtained by using measured data of the size-dependent soluble fractions of elements (e.g., Lindberg and Harriss, 1983). This procedure gave the mass fraction of the metal ions. From electroneutrality, it is derived that the coarse mode particles are also acidic. Acidic coarse particles have been measured, e.g., by Harrison and Pio (1981).

To evaluate the mean dry density of the particulate material, the water-insoluble fraction of the elements was assumed to be present as oxides for both data sets. This assumption is usually made when aerosol mass is accounted from elemental measurements (e.g., Stelson and Seinfeld, 1981). The densities of the oxides were taken from the Handbook of Chemistry and Physics (1986) (Table 2). For organic carbon, a density of 1.4 g/cm^3 and for elemental carbon a density of 2 g/cm^3 were used (Sloane, 1984).

The values for B^o and ρ_o obtained for the two cases (Fig. 2) are in the same range as activation parameters and dry densities measured by Hänel (1976) and Hänel and Lehmann (1981).

The assumptions made to obtain the concen-

Table 2. *Dry densities of insoluble substances*

	Densities (g/cm^3)		Densities (g/cm^3)
Al_2O_3	3.97	ZnO	5.61
SiO_2	2.65	MnO	5.43
Fe_2O_3	5.24	CuO	6.40
Na_2O	2.27	Cr_2O_3	5.21
K_2O	2.32	TiO_2	4.20
MgO	3.58	EC	2.00
CaO	3.25	OC	1.40
PbO	8.00		

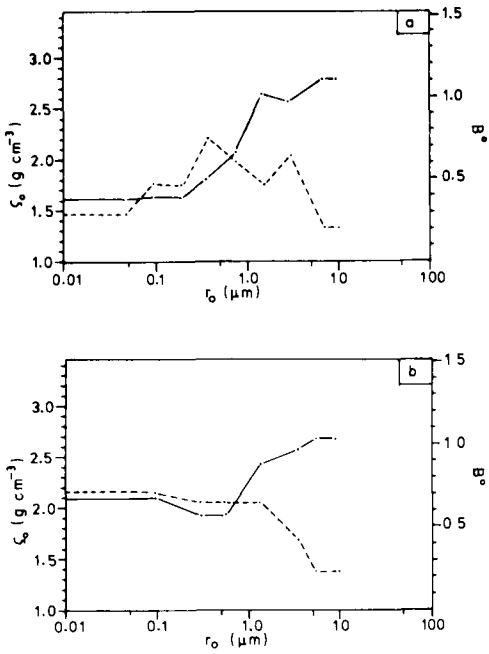

Fig. 2. Dry density ρ_o and activation parameter B^o plotted against the dry volume equivalent radii r_o of the aerosol particles used as input data for the model. ——: dry density ρ_o. – – –: activation parameter B^o. (a) Case A, mixed dataset Greppen/Wetterau. (b) Case B, dataset Solling.

Table 3. *Comparison of densities and activation parameter evaluated from substances—ions/elements*

	Densities (g/cm³)				
	Substances		Ions/elements		
	ρ_o	B^o	ρ_o	B^o	Chemical data from
Denver					Davis (1984)
fine	2.04	0.23	1.95	0.24	
coarse	2.68	0.11	2.84	0.10	
East Helena					Davis and Maugham (1984)
fine	2.51	0.29	2.98	0.30	
coarse	2.81	0.05	2.95	0.09	

trations of the substances from the elemental concentrations introduced an uncertainty in the dry densities and the activation parameter. To test the procedure, a comparison was made for 2 sets of aerosol composition for which both the concentrations of salts and minerals and the concentrations of elements are available. Davis (1984) and Davis and Maugham (1984) measured the concentrations of salts and minerals by X-ray diffraction on aerosol samples from Denver and East Helena. From the tabulated elemental contents of the minerals (Deer et al., 1963), the authors determined the elemental composition of the particles. The values for the mean density and the activation parameter were calculated directly from the concentrations of salts and minerals and were then compared with values obtained from the elemental composition by using the procedure described above (Table 3). The comparison showed deviations up to 10% for the Denver case for both the activation parameter and the mean dry density. In the case of East Helena, larger deviations occurred for the density of the fine particles and the activation parameter of the coarse particles. This aerosol was sampled near anthropogenic sources and contained a large amount of heavy metals like Zn and Cu. For such a case, the evaluation of the dry density and the activation parameter from the ions/elements seems to give larger errors.

The gas-phase concentrations of SO_2 ($3.5 \cdot 10^{-9}$ atm), O_3 ($3.4 \cdot 10^{-8}$ atm) and H_2O_2 ($1.9 \cdot 10^{-9}$ atm) were taken from measurements of Heikes et al. (1987) over eastern USA. For CO_2, a value of $3.3 \cdot 10^{-4}$ atm is assumed.

4. Chemical model

The concentrations of ions and catalytic active metals were calculated from the radii of the cloud droplets or interstitial particles, the dry volume equivalent radii and the mass fractions of the respective ions or metals. This was done for Na^+, K^+, Ca^{2+}, Mg^{2+}, NH_4^+, NO_3^-, Cl^-, total sulfate and the metals Fe and Mn. Then, the pH-value, the liquid phase concentrations of the trace gases in the droplets, the soluble part of the catalytic active metals and finally the initial oxidation rates of S(IV) were calculated. In the following section, the method of the calculation is described.

First, for all individual particle classes, the pH-values and the relevant ionic concentrations were calculated by holding the pressure of SO_2 constant. From the condition of electroneutrality (Table 4), the concentration of H^+ was determined by an iterative scheme considering the equilibria listed in Table 5. The charges of the ions, which were not explicitly considered in the equilibrium equations (e.g., Cl^-, Na^+, ...), were combined in the term $\sum_{ion}$. In this study, ammonium was also included in this term, although the formalism is able to describe the equilibrium between ammonium and ammonia. This was done because the mass fractions of NH_4^+ in the individual particle classes have been derived from the measured values. These mass fractions should not be changed in this case study. By considering equilibrium between NH_3 and the NH_4^+ concentrations in the particles, these mass fractions would have been changed in relation to the NH_3 pressure assumed.

In cases of large droplets in which the oxidation rate of S(IV) is limited by gas phase diffusion, the concentrations of SO_2(aq.), HSO_3^- and SO_3^{2-} are set to zero. It is assumed, that the droplets are well-mixed and that all dissolved S(IV) has reacted when the liquid phase reaction is faster than the gas phase diffusion of SO_2.

Table 4. *Conservation of mass and condition of electroneutrality*

Liquid phase:

Mass budgets:

$$[S(VI)] = [SO_4^{2-}] + [HSO_4^-]$$
$$[Fe_T] = [Fe(OH)_3] + [Fe^{3+}]$$
$$[Mn_T] = [Mn(OH)_2] + [Mn^{2+}]$$

Condition of electroneutrality:

$$[H^+] + [NH_4^+] + 2[Mn^{2+}] + 3[Fe^{3+}] + [\Sigma_{ion}] = [HSO_3^-] + 2[SO_3^{2-}] + [HSO_4^-] + 2[SO_4^{2-}] + [HCO^-] + 2[CO_3^{2-}] + [OH^+]$$

Parcel:

$$O_{3,T} = \frac{p_{O_3}}{RT} + L[O_3(aq.)]$$

$$H_2O_{2,T} = \frac{p_{H_2O_2}}{RT} + L[H_2O_2(aq.)]$$

$$S_T = \frac{p_{SO_2}}{RT} + \sum_j L_j([SO_2(aq.)]_j + [HSO_3^-]_j + [SO_3^{2-}]_j + [HSO_4^-]_j + [SO_4^{2-}]_j)$$

$$N_T = \frac{p_{NH_3}}{RT} + \sum_j L_j([NH_3(aq.)]_j + [NH_4^+]_j)$$

$$C_T = \frac{p_{CO_2}}{RT} + \sum_j L_j([CO_2(aq.)]_j + [HCO_3^-]_j + [CO_3^{2-}]_j)$$

No activity coefficients were considered together with the ionic concentrations. This could be done because the concentrations of the ions were generally very small. Only for the interstitial particles, and in some cases also for the large droplets, were the concentrations of the order of magnitude 0.1 to 1 moles/l. In this range, an activity correction may change the equilibria to some extent. However, for the interstitial particles, the sulfate production is small and in the large droplets, the oxidation rate of S(IV) is transport-limited as described later. Thus, it can be assumed that the sulfate production rate in the parcel will not change very much by using the activity correction.

When the ionic concentrations have been established for all size classes, the pressure of SO_2 was adjusted so that the sulfur mass was conserved. This was also reached by an iterative loop, because SO_2 dissolves in the droplets, dependent on pH-value. The same was done for CO_2 and has to be done for NH_3 if it is to be considered in the model calculations.

After establishing the concentrations of the ions and the conservation of the S(IV) mass, the oxidation rates of sulfur(IV) to sulfur(VI) were calculated by using the rate equations listed in Table 6. Here, the oxidation due to ozone, hydrogen peroxide and due to oxygen by the catalysts iron and manganese, was considered.

To test the assumption of equilibrium between gas and liquid phase, 4 characteristic times according to Schwartz and Freiberg (1981) are evaluated: $\tau_{c.a.}$ is the characteristic time associated with the chemical reaction of the substance c

Table 5. *Equilibrium conditions*

$[SO_2(aq.)] = K_1 p_{SO_2}$	$K_1 = 3.13 \cdot 10^{-5} \exp(3155/T)$	Hoffmann and Calvert (1985)
$[HSO_3^-] \cdot [H^+] = K_2 [SO_2(aq.)]$	$K_2 = 1.9 \cdot 10^{-5} \exp(2022/T)$	Tremblay and Leighton (1986)
$[SO_3^{2-}] \cdot [H^+] = K_3 [HSO_3^-]$	$K_3 = 2.3 \cdot 10^{-10} \exp(1671/T)$	Tremblay and Leighton (1986)
$[SO_4^{2-}] \cdot [H^+] = K_4 [HSO_4^-]$	$K_4 = 2.57 \cdot 10^{-6} \exp(2473/T)$	Hennes (1983)
$[Fe^{3+}] \cdot [OH^-]^3 = K_5$	$K_5 = 1.58 \cdot 10^{-39}$	Hoffmann and Calvert (1985)
$[H^+] \cdot [OH^-] = K_6$	$K_6 = 1.69 \cdot 10^{-24} \exp(6707/T)$	Hoffmann and Calvert (1985)
$[H_2O_2(aq.)] = K_7 p_{H_2O_2}$	$K_7 = 1.97 \cdot 10^{-7} \exp(7920/T)$	Hwang and Dasgupta (1985)
$[O_3(aq.)] = K_8 p_{O_3}$	$K_8 = 3.1 \cdot 10^{-6} \exp(2389/T)$	Hoffmann and Calvert (1985)
$[Mn^{2+}] \cdot [OH^-]^2 = K_9$	$K_9 = 1.58 \cdot 10^{-13}$	Hoffmann and Calvert (1985)
$[NH_3(aq.)] = K_{10} p_{NH_3}$	$K_{10} = 6.08 \cdot 10^{-5} \exp(4107/T)$	Hoffmann and Calvert (1985)
$[NH_4^+] \cdot [OH^-] = K_{11} [NH_3(aq.)]$	$K_{11} = 1.8 \cdot 10^{-5}$	Tremblay and Leighton (1986)
$[CO_2(aq.)] = K_{12} p_{CO_2}$	$K_{12} = 3.16 \cdot 10^{-2}$	Stumm et al. (1987)
$[HCO_3^-] \cdot [H^+] = K_{13} [CO_2(aq.)]$	$K_{13} = 5.01 \cdot 10^{-7}$	Stumm et al. (1987)
$[CO_3^{2-}] \cdot [H^+] = K_{14} [HCO_3^-]$	$K_{14} = 6.31 \cdot 10^{-11}$	Stumm et al. (1987)

Table 6. *Oxidation rates*

Hydrogen peroxide:	
$\frac{d[S(VI)]}{dt} = \frac{80000 \exp(-3650/T + 12.2483) \cdot [H_2O_2(aq.)] \cdot [SO_2(aq.)]}{0.1 + [H^+]}$	Martin (1984)
Ozone:	
$\frac{d[S(VI)]}{dt} = \{4.39 \cdot 10^{11} \exp(-4131/T) + 2560 \exp(966/T)/[H^+]\} \cdot [S(IV)] \cdot [O_3(aq.)]$	Maahs (1983)
iron–manganese synergism:	
$\frac{d[S(VI)]}{dt} = 5.83 \cdot 10^{19} \cdot [H^+]^{-0.74} \cdot [Fe^{3+}] \cdot [Mn^{2+}] \cdot [S(IV)] \exp(-8431/T)$ for pH $\leqslant 4.2$	Ibusuki and Takeuchi (1987)
$\frac{d[S(VI)]}{dt} = 5.38 \cdot 10^{25} \cdot [H^+]^{0.67} \cdot [Fe^{3+}] \cdot [Mn^{2+}] \cdot [S(IV)] \exp(-8431/T)$ for pH > 4.2	

in the liquid phase:

$$\tau_{c.a.}^{-1} = -\frac{1}{[c]} \cdot \frac{d[c]}{dt}. \tag{7}$$

This characteristic time is defined for a first-order reaction. The S(IV) oxidation can be considered as a pseudo-first-order reaction only if O_3 and H_2O_2 are present in excess throughout the droplet. This assumption does not hold in every case as will be described later. However, the characteristic time can be used to estimate which processes have to be considered.

τ_{reag} is the characteristic time required for gas-phase diffusion to supply an amount of reagent to the droplet necessary to produce a concentration of dissolved reagent in equilibrium with the bulk gas-phase reagent concentration:

$$\tau_{reag} = \tfrac{1}{3} r^2 D_g \eta H R T, \tag{8}$$

with D_g the diffusion constant in the gas phase and H the Henry-law constant of the specific gas. η is a correction factor which describes the dissociation of the dissolved gas in the liquid phase, e.g., for S(IV), η is the ratio between the total concentration of S(IV) in the liquid phase and the concentration of the dissolved SO_2(aq.). R is the universal gas constant and T the absolute temperature.

Two other characteristic times have been evaluated: $\tau_{d.a.}$, the characteristic time associated with the diffusion of the dissolved gas in the liquid phase

$$\tau_{d.a.} = r^2 \pi^{-2} D_a^{-1}, \tag{9}$$

with D_a the molecular diffusion constant of the dissolved gas in the liquid phase. For this, it is assumed that no internal circulation is present in the small cloud droplets, and that the dissolved gas is transported by molecular diffusion only. $\tau_{d.g.}$ is the characteristic time associated with the diffusion in the gas phase:

$$\tau_{d.g.} = r^2 \pi^{-2} D_g^{-1}. \tag{10}$$

Because limitation of the reaction rate by gas phase diffusion was found for some droplet classes, the chemical reaction rates were compared with the rate of increase of the reagent concentrations by gas-phase diffusion. The gas-phase diffusion of reagents to the surface of the droplet is set to maximum, because the concentrations of the dissolved gases were set to zero (see above) and therefore, they have no saturation pressure above the surface of the droplet:

$$\frac{dc}{dt} = \frac{4\pi r D_g}{ML} \rho_g, \tag{11}$$

with M the molecular mass of the reactant, L the volume of the electrolyte solution of the droplet and ρ_g the gas phase density of the reactant.

The velocity of the reaction is limited either by the liquid phase S(IV) oxidation rate or by the rate of reagent supply by gaseous transport. Thus, the real rate is the minimum of both rates for each reactant O_3, H_2O_2 and O_2. The oxidation rate of S(IV) is the minimum of the sum of the individual rates and the rate of supply of SO_2 by

gas-phase diffusion:

$$\frac{d[S(IV)]}{dt} = \min\left\{\left[\min\left(\frac{d[S(IV)]|_{O_3}}{dt}, \frac{d[O_3]_{trnsp}}{dt}\right) + \min\left(\frac{d[S(IV)]|_{H_2O_2}}{dt}, \frac{d[H_2O_2]_{trnsp}}{dt}\right) + \min\left(\frac{d[S(IV)]|_{Mn+Fe}}{dt}, \frac{d[O_2]_{trnsp}}{dt}\right)\right], \frac{d[SO_2]_{trnsp}}{dt}\right\}. \quad (12)$$

In the case where the reaction is limited by SO_2 transport, the apportionment of the sulfate production to the individual oxidants is the same as if there were no transport limitation.

To obtain the total oxidation rate for the whole parcel, the oxidation rates of the individual droplets were summed up, and weighted by the volumes of the electrolyte solution of the individual droplets.

5. Results

The size distribution of the aerosol particles at the start of the model calculations is shown in Fig. 3a for case A and in Fig. 4a for case B. By integration of the size distributions, the number concentrations of the aerosol particles are obtained which are 3237 particles/cm^3 for case A and 5526 particles/cm^3 for case B. Such concentrations are typical for rural, continental aerosol. The equilibrium radii at the start of the model are calculated from eq. (1). This formula gives only approximate values at relative humidities below 100%. It can be used, because the equilibrium radii are used for the initialization of the model only and at higher relative humidities, eq. (1) gives more accurate values.

The initial temperature is 8.7°C. By adiabatic cooling, the parcel has a temperature of 0°C at the cloud base.

In the cloud, the size distribution is split up into the growing droplets and the interstitial particles. In Figs. 3b and 4b, the size distributions are shown at the end of the model calculation (approximately 370 m above the cloud base), for an updraft velocity of 1 m/s. At this height above cloud base, the maximum relative humidity in the cloud has been passed, no more smaller particles are activated and therefore, the cloud droplet concentration has reached a stable

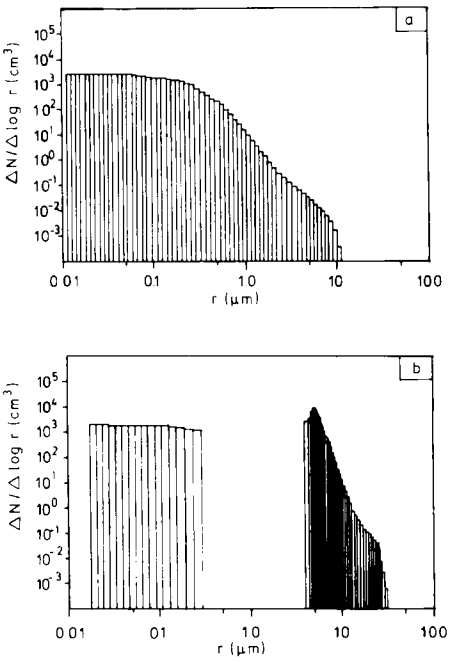

Fig. 3. Size distribution of aerosol particles and droplets for case A, mixed dataset Greppen/Wetterau. (a) Size distribution of aerosol particles at 60% relative humidity. All particles are in equilibrium with the ambient relative humidity at the start of the model calculation. (b) Size distribution of interstitial particles (left) and cloud droplets (right) at a level approximately 370 m above the cloud base (end of the model calculation). In the cloud, the activated droplets have grown rapidly and have reached radii of approximately 5 μm. The interstitial particles are in equilibrium with the ambient relative humidity. They are smaller than 0.4 μm.

value. At a greater height, entrainment is more likely than near the cloud base. Then, a closed parcel model is not adequate for description of the microphysical processes exactly. The updraft velocity of 1 m/s was chosen, because then the results of the chemical model are most applicable. At a higher updraft velocity, the residence time of the parcel near the cloud base is too small for production of a considerable amount of sulfate, and at a greater height, entrainment should be considered, as mentioned above. At a smaller updraft velocity, the large droplets have high sedimentation velocities and the sedimentation of the droplets cannot be described in a closed-

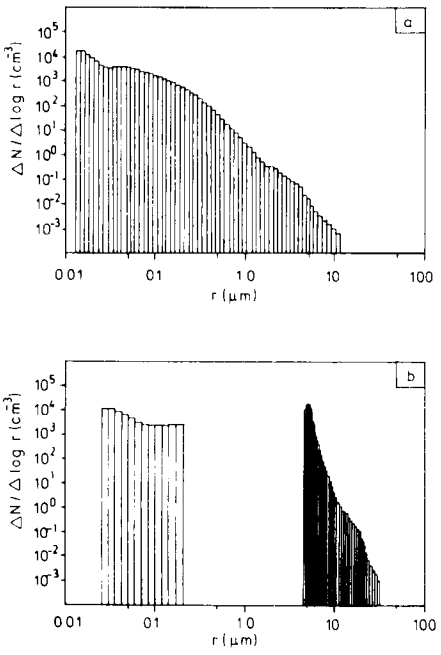

Fig. 4. Same as Fig. 3, but for case B, dataset Solling.

parcel model. The mean radii of the cloud droplets in both cases are approximately 5 μm, a value typically found during measurements near the cloud base (Diem, 1948; Blyth and Latham, 1985). In both cases, nearly the same concentration of growing droplets has established: 1068 cm^{-3} for case A and 1112 cm^{-3} for case B. The number concentration of droplets and their mean radius depend on the updraft velocity and the aerosol type (Hänel, 1987).

Figs. 5, 6 show the apportionment of the liquid water and the dry particulate mass to the individual size classes. For example, if one of the histogram bars reaches 0.1, then 10% of the liquid water, or of the dry particulate mass per unit volume, is in this size class. At the beginning of the model calculations, the deviations between the apportionment of the dry mass and the liquid water are caused by the different activation parameters of the small and large particles (Figs. 5a, 6a). The absolute liquid water content is very small: $4.6 \cdot 10^{-5}$ g/m^3 for case A and $1.6 \cdot 10^{-5}$ g/m^3 for case B. But one should bear in mind that these values are derived from the particle radii, which are calculated from the approximate eq. (1).

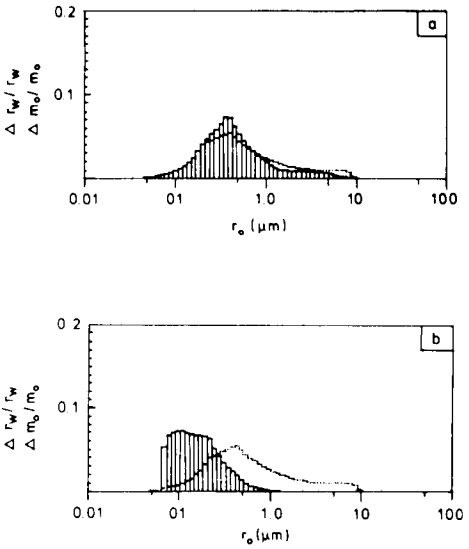

Fig. 5. Apportionment of the dry particulate mass m_o and the liquid water mixing ratio r_w to the particle size classes: $\Delta m_o/m_o$ and $\Delta r_w/r_w$ as functions of the volume equivalent radius r_o of the particles for case A, mixed dataset Greppen/Wetterau. ——: $\Delta r_w/r_w$. ·····: $\Delta m_o/m_o$. (a) Apportionment at 60% relative humidity (start of the model calculation). (b) Apportionment at a level approximately 370 m above the cloud base (end of the model calculation).

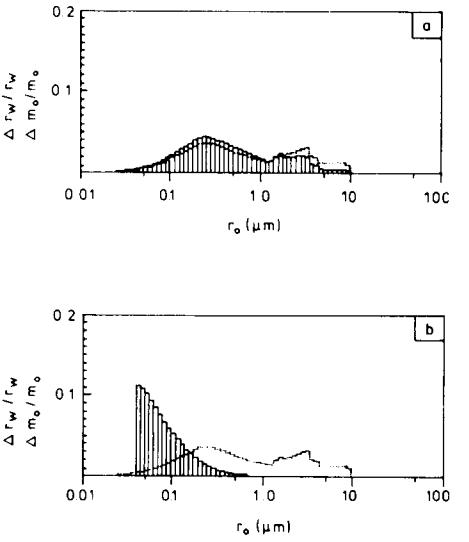

Fig. 6. Same as Fig. 5, but for case B, dataset Solling.

At the end of the model calculations, the situation is totally different. The liquid water content is 0.56 g/m^3 for case A and 0.55 g/m^3 for case B. Most of the liquid water is on the activated droplets which have grown by an order of magnitude or more from their initial radius (compare Figs. 3b, 4b). The growth rate of the larger droplets was limited by diffusion of water vapor to their surface. Therefore, the radius of the largest droplets, for example, has increased only by a factor of 3. The interstitial particles have also not grown very much. In the cloud, they still are in equilibrium with the relative humidity of the surrounding air.

Consequently, we get the following picture of the concentrations of ions and metals (Table 7). In the interstitial particles (classes no. 1 and 10), sulfate, nitrate and ammonium have high concentrations, of the order of 0.1 to 1 moles/l. On the small, activated droplets (class no. 20), minimum concentrations of ions and metals are found, due to the high ratio between the liquid water mass and the mass of the dry particulate material. The concentrations of sulfate, nitrate and ammonium are in the range 10^{-6} to 10^{-4} moles/l. Iron and manganese have concentrations of the order of 10^{-8} and 10^{-7} moles/l. The small concentrations of the catalytic active metals have the consequence, that the catalytic oxidation of S(IV) is not important in the activated droplets as is discussed later. Due to the smaller growth rates of the large droplets, the ions have higher concentrations in these droplets, of the order of 10^{-2} moles/l for sulfate and nitrate in the largest droplets.

These concentrations are taken as input data for the chemical model. In both cases, the pH-values are very different for the different sized droplets. In Table 7, the pH-values for equilibrium between gas and liquid phase are listed. The interstitial particles are generally acidic. In case A, one class of the interstitial particles is initially

Table 7. *Concentrations of ions and catalytic active metals*

Concentrations (moles/l)							
Case A: mixed dataset Greppen/Wetterau							
class	1	10	20	30	40	50	60
r_o (μm)	0.0106	0.0299	0.0944	0.299	0.944	2.99	9.44
r (μm)	0.0187	0.0834	4.93	6.44	10.0	19.1	30.5
SO_4^{2-} [1]	$5.9\cdot10^{-1}$	$1.4\cdot10^{-1}$	$1.2\cdot10^{-5}$	$4.0\cdot10^{-4}$	$2.5\cdot10^{-3}$	$2.7\cdot10^{-3}$	$1.7\cdot10^{-2}$
NO_3^-	$1.6\cdot10^{0}$	$3.8\cdot10^{-1}$	$5.3\cdot10^{-5}$	$1.3\cdot10^{-3}$	$6.6\cdot10^{-3}$	$1.3\cdot10^{-2}$	$3.5\cdot10^{-2}$
Cl^-	—	—	$7.2\cdot10^{-9}$	$2.5\cdot10^{-5}$	$9.1\cdot10^{-5}$	—	—
NH_4^+	$2.4\cdot10^{0}$	$5.7\cdot10^{-1}$	$1.3\cdot10^{-4}$	$1.3\cdot10^{-3}$	$1.2\cdot10^{-2}$	$8.9\cdot10^{-3}$	$4.6\cdot10^{-2}$
Fe	$5.7\cdot10^{-3}$	$1.4\cdot10^{-3}$	$2.1\cdot10^{-7}$	$2.0\cdot10^{-5}$	$1.0\cdot10^{-3}$	$6.0\cdot10^{-3}$	$7.5\cdot10^{-2}$
Mn	$5.7\cdot10^{-4}$	$1.4\cdot10^{-4}$	$2.1\cdot10^{-8}$	$1.6\cdot10^{-8}$	$3.9\cdot10^{-5}$	$1.7\cdot10^{-4}$	$1.7\cdot10^{-3}$
pH	1.43	1.62	5.39	3.17	6.81	7.55	7.71
Case B: Solling							
class	1	10	20	30	40	50	60
r_o (μm)	0.0106	0.0299	0.0944	0.299	0.944	2.99	9.44
r (μm)	0.0275	0.131	5.35	6.58	10.3	18.2	31.3
SO_4^{2-} [1]	$3.9\cdot10^{-1}$	$7.3\cdot10^{-2}$	$3.3\cdot10^{-5}$	$5.6\cdot10^{-4}$	$3.3\cdot10^{-3}$	$8.4\cdot10^{-3}$	$1.7\cdot10^{-2}$
NO_3^-	$1.4\cdot10^{-2}$	$2.8\cdot10^{-3}$	$1.3\cdot10^{-6}$	$5.7\cdot10^{-5}$	$1.3\cdot10^{-3}$	$1.3\cdot10^{-2}$	$4.4\cdot10^{-2}$
Cl^-	$1.8\cdot10^{-2}$	$3.6\cdot10^{-3}$	$1.7\cdot10^{-6}$	$1.4\cdot10^{-5}$	$2.2\cdot10^{-4}$	$2.6\cdot10^{-3}$	$1.8\cdot10^{-2}$
NH_4^+	$5.0\cdot10^{-1}$	$9.5\cdot10^{-2}$	$4.2\cdot10^{-5}$	$1.1\cdot10^{-3}$	$7.0\cdot10^{-3}$	$3.6\cdot10^{-3}$	—
Fe	$2.5\cdot10^{-3}$	$4.9\cdot10^{-4}$	$2.3\cdot10^{-7}$	$6.8\cdot10^{-6}$	$2.3\cdot10^{-5}$	$6.3\cdot10^{-5}$	$5.4\cdot10^{-4}$
Mn	$6.2\cdot10^{-4}$	$1.2\cdot10^{-4}$	$5.6\cdot10^{-8}$	$1.2\cdot10^{-6}$	$1.6\cdot10^{-5}$	$5.5\cdot10^{-5}$	$4.5\cdot10^{-4}$
pH	1.23	1.49	4.21	3.91	2.71	1.24	0.69

[1] Total sulfate ($[SO_4^{2-}] + [HSO_4^-]$).

basic and would have a pH-value of 6.9. The activated droplets are also acidic, but because of the high dilution of the electrolyte solutions, the pH-values are in the range from 4 to 5. They are influenced in part by the solution of the gases SO_2 and CO_2 into the droplets. But still, the composition of the aerosol particles, which had acted as condensation nuclei, has an influence to the pH-value of the activated droplet (compare class no. 20 in Table 8 for cases A and B).

The pH-values of the larger droplets depend strongly on the composition of the coarse aerosol particles. They can contain a large amount of nitrate and may be acidic, as in case B. Then the droplets are acidic, too, and due to relative high concentrations of the electrolyte solutions, the pH-values are below 2. If the large aerosol particles are initially basic as in case A, by equilibrium between gas and liquid phase, large amounts of SO_2 and CO_2 dissolve into the droplets. Therefore, the pH-value decreases to values near 7. But for SO_2, no equilibrium exists because of the fast oxidation in these droplets, as is discussed later.

In Table 8, the characteristic times (eqs. (7)–(10)) are listed together with the sulfate production rates under two conditions: first, equilibrium between gas phase and liquid phase for SO_2, O_3 and H_2O_2, and second the reaction rate according to eq. (12), where transport

Table 8. *Oxidation rates of sulfur(IV) and characteristic times*

Case A: mixed dataset Greppen/Wetterau							
class	1	10	20	30	40	50	60
r_o (μm)	0.0106	0.0299	0.0944	0.299	0.944	2.99	9.44
r (μm)	0.0187	0.0834	4.93	6.44	10.0	19.1	30.5
τ_{reag} [3]							
O_3	$4.4\cdot10^{-12}$	$8.7\cdot10^{-11}$	$3.0\cdot10^{-7}$	$5.2\cdot10^{-7}$	$1.3\cdot10^{-6}$	$4.5\cdot10^{-6}$	$1.2\cdot10^{-5}$
H_2O_2	$2.1\cdot10^{-4}$	$4.2\cdot10^{-3}$	$1.5\cdot10^{+1}$	$2.5\cdot10^{+1}$	$6.0\cdot10^{+1}$	$2.2\cdot10^{+2}$	$5.6\cdot10^{+2}$
S(IV)	$1.5\cdot10^{-9}$	$3.7\cdot10^{-8}$	$4.4\cdot10^{-1}$	$4.8\cdot10^{-3}$	$8.0\cdot10^{+1}$	$4.5\cdot10^{+3}$	$2.3\cdot10^{+4}$
$\tau_{c.a.}$ [3]							
O_3	$7.2\cdot10^{+2}$	$5.7\cdot10^{+2}$	$1.0\cdot10^{-3}$	$1.3\cdot10^{+1}$	$8.6\cdot10^{-7}$	$1.0\cdot10^{-8}$	$3.5\cdot10^{-9}$
H_2O_2	$8.7\cdot10^{+2}$	$8.0\cdot10^{+2}$	$6.5\cdot10^{+2}$	$6.5\cdot10^{+2}$	$6.5\cdot10^{+2}$	$6.5\cdot10^{+2}$	$6.5\cdot10^{+2}$
S(IV)	$1.3\cdot10^{-2}$	$7.0\cdot10^{-2}$	$6.2\cdot10^{+1}$	$1.9\cdot10^{0}$	$3.0\cdot10^{0}$	$5.4\cdot10^{-1}$	$3.7\cdot10^{-1}$
$\tau_{d.a.}$ [3]	$2.0\cdot10^{-8}$	$3.9\cdot10^{-7}$	$1.4\cdot10^{-3}$	$2.3\cdot10^{-3}$	$5.7\cdot10^{-3}$	$2.0\cdot10^{-2}$	$5.2\cdot10^{-2}$
$\tau_{d.g.}$	$2.8\cdot10^{-12}$	$5.6\cdot10^{-11}$	$1.9\cdot10^{-7}$	$3.3\cdot10^{-7}$	$8.1\cdot10^{-7}$	$2.9\cdot10^{-6}$	$7.5\cdot10^{-6}$
Equilibrium							
pH	1.43	1.62	5.39	3.17	6.81	7.55	7.71
$\frac{dS(VI)}{dt}$ [2]	$1.5\cdot10^{-7}$	$1.5\cdot10^{-7}$	$9.0\cdot10^{-7}$	$1.9\cdot10^{-7}$	$8.4\cdot10^{-4}$	$7.1\cdot10^{-2}$	$2.1\cdot10^{-1}$
by							
Fe + Mn	0.081	0.009	<0.001	<0.001	<0.001	<0.001	<0.001
O_3	<0.001	<0.001	0.793	<0.001	1.000	1.000	1.000
H_2O_2	0.919	0.991	0.207	1.000	<0.001	<0.001	<0.001
Transport limitation							
pH	1.43	1.62	7.01	3.17	8.79	9.85	10.04
$\frac{dS(VI)}{dt}$ [2]	$2.8\cdot10^{-7}$	$2.9\cdot10^{-7}$	$9.3\cdot10^{-7}$	$3.5\cdot10^{-7}$	$2.3\cdot10^{-5}$	$6.2\cdot10^{-6}$	$2.5\cdot10^{-6}$
by							
Fe + Mn	0.081	0.009	<0.001	<0.001	<0.001	<0.001	<0.001
O_3	<0.001	<0.001	1.000	<0.001	0.999	0.996	0.989
H_2O_2	0.919	0.991	<0.001	1.000	0.001	0.004	0.011

limitation in the gas phase is included. The pH-values under both conditions are also listed.

The characteristic time $\tau_{c.a.}$ depends on the reaction rate and the concentration of the reagent. Consequently, the characteristic times $\tau_{c.a.}$ are very different for ozone, hydrogen peroxide and S(IV). For ozone, $\tau_{c.a.}$ is small for basic droplets because the reaction rate with S(IV) is large and the liquid phase concentration of ozone is small. The liquid phase concentration of H_2O_2 is larger by orders of magnitude than the concentration of ozone, and the reaction rate with S(IV) is smaller. Therefore, $\tau_{c.a.}$ for the reaction of H_2O_2 is between 650 and 850 s. For S(IV), the liquid phase concentration as well as the reaction rate depend very much upon the pH-value of the droplet and the concentrations of the oxidants. However, for the droplets with high pH-values, this characteristic time is larger for S(IV) than for ozone caused by the higher liquid phase concentrations of S(IV). For ozone and hydrogen peroxide, τ_{reag} is independent of the pH-value. For these reagents, it depends only on the droplet radius and increases with increasing

Table 8—*continued*

Case B: Solling							
class	1	10	20	30	40	50	60
r_o (μm)	0.0106	0.0299	0.0944	0.299	0.944	2.99	9.44
r (μm)	0.0275	0.131	5.35	6.58	10.3	18.2	31.3
τ_{reag} [3]							
O_3	$9.8\cdot10^{-12}$	$1.8\cdot10^{-7}$	$2.0\cdot10^{-7}$	$2.6\cdot10^{-7}$	$5.6\cdot10^{-7}$	$1.7\cdot10^{-6}$	$5.5\cdot10^{-6}$
H_2O_2	$4.8\cdot10^{-4}$	$8.8\cdot10^{0}$	$9.6\cdot10^{0}$	$1.2\cdot10^{+1}$	$2.7\cdot10^{+1}$	$8.3\cdot10^{+1}$	$2.6\cdot10^{+2}$
S(IV)	$2.7\cdot10^{-9}$	$4.7\cdot10^{-2}$	$8.6\cdot10^{-3}$	$4.6\cdot10^{-3}$	$8.2\cdot10^{-4}$	$3.5\cdot10^{-4}$	$9.9\cdot10^{-4}$
$\tau_{c.a.}$ [3]							
O_3	$5.2\cdot10^{+2}$	$1.7\cdot10^{-2}$	$5.3\cdot10^{-1}$	$2.6\cdot10^{0}$	$8.7\cdot10^{+1}$	$7.2\cdot10^{+2}$	$8.1\cdot10^{+2}$
H_2O_2	$5.8\cdot10^{+2}$	$3.8\cdot10^{+2}$	$3.8\cdot10^{+2}$	$3.8\cdot10^{+2}$	$4.0\cdot10^{+2}$	$1.1\cdot10^{+3}$	$3.1\cdot10^{+3}$
S(IV)	$1.1\cdot10^{-2}$	$4.8\cdot10^{+1}$	$9.0\cdot10^{0}$	$3.4\cdot10^{0}$	$1.9\cdot10^{-1}$	$1.0\cdot10^{-1}$	$2.0\cdot10^{-2}$
$\tau_{d.a.}$ [3]	$4.4\cdot10^{-8}$	$8.2\cdot10^{-4}$	$8.9\cdot10^{-6}$	$1.2\cdot10^{-3}$	$2.5\cdot10^{-3}$	$7.8\cdot10^{-3}$	$2.5\cdot10^{-2}$
$\tau_{d.g.}$	$6.4\cdot10^{-12}$	$1.2\cdot10^{-7}$	$1.3\cdot10^{-7}$	$1.7\cdot10^{-7}$	$3.6\cdot10^{-7}$	$1.1\cdot10^{-6}$	$3.5\cdot10^{-6}$
Equilibrium							
pH	1.23	1.49	4.21	3.91	2.71	1.24	0.69
$\frac{dS(VI)}{dt}$ [2] by	$3.1\cdot10^{-7}$	$2.5\cdot10^{-7}$	$3.3\cdot10^{-7}$	$3.2\cdot10^{-7}$	$3.2\cdot10^{-7}$	$2.1\cdot10^{-7}$	$2.3\cdot10^{-7}$
Fe + Mn	0.344	0.030	<0.001	<0.001	<0.001	0.027	0.549
O_3	<0.001	<0.001	0.018	0.005	<0.001	<0.001	<0.001
H_2O_2	0.656	0.970	0.982	0.995	1.000	0.973	0.451
Transport limitation							
pH	1.23	1.49	4.21	3.91	2.71	1.24	0.69
$\frac{dS(VI)}{dt}$ [2] by	$3.2\cdot10^{-7}$	$2.6\cdot10^{-7}$	$3.4\cdot10^{-7}$	$3.4\cdot10^{-7}$	$3.3\cdot10^{-7}$	$2.2\cdot10^{-7}$	$2.5\cdot10^{-7}$
Fe + Mn	0.344	0.030	<0.001	<0.001	<0.001	0.027	0.549
O_3	<0.001	<0.001	0.018	0.005	<0.001	<0.001	<0.001
H_2O_2	0.656	0.970	0.982	0.995	1.000	0.973	0.451

[1] Total sulfate ($[SO_4^{2-}] + [HSO_4^-]$).
[2] moles l^{-1} s^{-1}.
[3] s.

radius. For S(IV), τ_{reag} also depends on the pH-value due to the pH-dependent dissociation. For droplets with high pH-values, τ_{reag} is very large because of the high liquid phase concentration necessary to maintain equilibrium with the gas phase. Therefore, τ_{reag} for S(IV) is of the order of 16,000 to 35,000 s for the largest, basic droplets.

The sulfate production rates are listed for equilibrium between gas and liquid phase and for transport limitation in the gas phase. As mentioned in Section 3, if the S(IV) reaction was limited by diffusion of SO_2, the liquid phase concentration of S(IV) was set to zero. This has two consequences: at first the pH-value is higher in these droplets (e.g., case A, classes 40 to 60) than in S(IV) equilibrium. The second consequence is due to the fact that the parcel is closed: the SO_2-pressure is higher, if no S(IV) dissolves in large droplets with high pH-values. Especially in case A, the difference is remarkable: p_{SO_2} is $3.48 \cdot 10^{-9}$ atm if transport limitation is considered. In the equilibrium case, the pressure is lowered to $1.83 \cdot 10^{-9}$ atm. Further, due to the higher SO_2 pressure, the sulfur production rates are higher in particle classes with no transport limitation, e.g., the interstitial particles (classes 1 and 10).

In the interstitial particles, sulfate is produced mainly by H_2O_2 and, to a smaller fraction, by the synergism of iron and manganese because of the high metal concentrations. The sulfur production rates are in the range of $1.5 \cdot 10^{-7}$ to $3.2 \cdot 10^{-7}$ moles l^{-1} s^{-1}. In case A, the initial basic class no. 16 of the interstitial particles has an initial sulfate production rate which is higher by orders of magnitude than the production rates of the other interstitial particles together (Table 9). However, this class could be acidic after a short time, because the sulfate production is not limited by gaseous transport (see below).

The activated droplets have higher pH-values than the acidic interstitial particles. Therefore, the oxidation of S(IV) by ozone also becomes important beside of the oxidation by hydrogen peroxide. Due to the small metal concentrations, the contribution of the catalytic oxidation by manganese and iron is not important. For acidic droplets, the sulfate production is not limited by gaseous diffusion because of the small size of the droplets. The production rates are not much different from the interstitial particles; they are still smaller than $9.3 \cdot 10^{-7}$ moles l^{-1} s^{-1}. Only for droplets with high pH-values in the basic range, is the reaction of S(IV) with ozone fast and therefore, is limited by gaseous diffusion of SO_2 (e.g., class no. 20 in case A). However, this size class is a borderline case. By an equilibrium liquid phase concentration of S(IV), the pH-value decreases to 5.39 and the reaction rate is not limited by gas phase transport.

If the large droplets are acidic, sulfate is produced in a similar way as in the interstitial particles (case B). The main contributions come from H_2O_2 and the iron–manganese synergism. If the droplets have high pH-values as in case A, S(IV) is mainly oxidized by the reaction with ozone. For equilibrium between gas and liquid phase of O_3 and SO_2, the production rate would be of the order of 10^{-2} moles l^{-1} s^{-1}. However, by comparing the characteristic times $\tau_{c.a.}$ and τ_{reag}, one can see that $\tau_{c.a.}$ is smaller by orders of magnitude than τ_{reag} for the largest basic droplets for ozone and S(IV). Therefore, the assumption of equilibrium between the gas and liquid phase

Table 9. *Time for doubling initial dry mass of aerosol particles by the initial sulfate production rate*

Class no.	Case	Initial pH-value	Initial S(VI)-prod. rate moles l^{-1} s^{-1}	Initial dry part. mass g	Volume of solution l	H_2SO_4-prod. rate g s^{-1}	Time for doubling init. mass s
15	A	2.40	$3.4 \cdot 10^{-7}$	$1.0 \cdot 10^{-15}$	$3.9 \cdot 10^{-17}$	$1.3 \cdot 10^{-21}$	791,000
16	A	9.10	$3.3 \cdot 10^{-2}$	$1.4 \cdot 10^{-15}$	$7.7 \cdot 10^{-17}$	$2.5 \cdot 10^{-16}$	5.9
20	A	7.01	$9.3 \cdot 10^{-5}$	$5.8 \cdot 10^{-15}$	$5.0 \cdot 10^{-13}$	$4.6 \cdot 10^{-15}$	1.3
20	B	4.21	$3.4 \cdot 10^{-7}$	$7.5 \cdot 10^{-15}$	$6.4 \cdot 10^{-13}$	$2.2 \cdot 10^{-17}$	344
50	A	9.85	$6.2 \cdot 10^{-6}$	$2.9 \cdot 10^{-10}$	$2.9 \cdot 10^{-11}$	$1.8 \cdot 10^{-14}$	16,400
50	B	1.24	$2.2 \cdot 10^{-7}$	$2.8 \cdot 10^{-10}$	$2.5 \cdot 10^{-11}$	$5.4 \cdot 10^{-16}$	525,000

Table 10. *Oxidation rates in total parcel. Sum of size classes and bulk cloud water*

$dS(VI)/dt$ (moles m^{-3} s^{-1})

		Size classes equilibrium	Size classes transp. ltd.	Bulk cloud water
Case A:	interstitial particles	$2.6 \cdot 10^{-11}$ [a]	$3.1 \cdot 10^{-10}$ [b]	
	activated droplets	$2.4 \cdot 10^{-10}$	$3.1 \cdot 10^{-8}$	
	large droplets	$8.0 \cdot 10^{-8}$	$3.2 \cdot 10^{-10}$	
	sum	$8.0 \cdot 10^{-8}$	$3.2 \cdot 10^{-8}$	$1.1 \cdot 10^{-9}$
	production by Fe + Mn	<0.001	<0.001	0.780
	O_3	0.998	0.996	0.005
	H_2O_2	0.002	0.004	0.215
	pH			4.27
Case B:	interstitial particles	$3.2 \cdot 10^{-15}$	$3.4 \cdot 10^{-15}$	
	activated droplets	$2.2 \cdot 10^{-10}$	$2.3 \cdot 10^{-10}$	
	large droplets	$1.0 \cdot 10^{-9}$ [c]	$4.3 \cdot 10^{-10}$ [d]	
	sum	$1.2 \cdot 10^{-9}$	$6.6 \cdot 10^{-10}$	$2.4 \cdot 10^{-10}$
	production by Fe + Mn	<0.001	<0.001	0.012
	O_3	0.828	0.664	0.004
	H_2O_2	0.172	0.336	0.985
	pH			3.85

Comments

Case A: size class 16 is initially basic. Sulfate production rate of interstitial particles without class 16:

[a] $2.0 \cdot 10^{-15}$ moles m^{-3} s^{-1}.

[b] $3.7 \cdot 10^{-15}$ moles m^{-3} s^{-1}.

Case B: size classes 32–39 have high pH-values and make the main contribution to the sulfate production of the large droplets:

[c] pH-values between 5.30 and 6.59, $dS(VI)/dt = 1.0 \cdot 10^{-9}$ moles m^{-3} s^{-1}, by O_3 0·996, by H_2O_2 0.004.

[d] pH-values between 7.16 and 7.84, $dS(VI)/dt = 4.3 \cdot 10^{-10}$ moles m^{-3} s^{-1}, by O_3 0·999, by H_2O_2 0.001.

is not valid for these droplets. The characteristic time of chemical reaction is much smaller than the time necessary to saturate the droplet with the reagent by gas-phase diffusion. The reaction is limited by the transport of both SO_2 and O_3 to the surface of the droplet. Therefore, the transport limited sulfate production rate is smaller by orders of magnitude than the rate for equilibrium (Table 8, case A).

Now, the sum of the sulfur production rates in all droplets in the parcel shall be considered (Table 10). Despite the similar oxidation rates per liquid water volume, with respect to the whole parcel more sulfate is produced in the larger liquid water volume of the droplets than in the interstitial particles. The absolute value of the initial sulfate production rate depends mainly on the pH-value of the individual droplets. If droplets with high pH-values are present, the initial rate is higher by up to 2 orders of magnitude. Then, the sum of the production rates of the individual droplet classes is higher than the oxidation rate calculated for the mean chemical position of the bulk cloud water.

6. Conclusions

In this study, the initial sulfate production rates in cloud droplets and interstitial particles are calculated from the given aerosol composition and the separately given gas pressures of SO_2, O_3 and H_2O_2. The result is that basic droplets considerably increase the initial sulfate production rate in the parcel. But then the question arises, of how long can the rate be as high as this because sulfuric acid is produced under the prevailing conditions (no NH_3) and therefore, the pH-value of the droplets and consequently, the sulfate production rates would be lowered. In

Table 9 for selected size classes, the time is calculated during which the mass of the dry particulate material is doubled by production of sulfuric acid. In case A, one class of interstitial particles is initially basic (no. 16). After 5.9 s, the mass of the produced sulfuric acid is equal to the mass of the initial dry aerosol particle. Then, the particle would be acidic and the sulfate production rate would be as low as for the particle class 15, which was initially acidic. For comparison, for this class, it would take 791,000 s to double the mass by sulfuric acid production, a time which is longer than the life-time of most cloud types in the atmosphere. For the activated cloud droplets (size class 20), the situation is similar. A basic droplet (as in case A) would be acidic in even a shorter time than a basic interstitial particle. However, an acidic droplet with a pH-value of approximately 4 would also produce a large amount of sulfuric acid, so that the mass of the dry particulate material is doubled within 344 s, a time comparable to the residence time of a small cumulus. This is caused by the large volume of the electrolyte solution, in which the sulfate production occurs, compared to the volume of the particulate material in a dry state. For the large droplets (class no. 50), transport limitation is effective if they are basic (as in case A). The result is that the sulfur production rate is only an order of magnitude higher than the one of acidic large droplets. Both times for doubling the initial mass are very long compared to the life-time of many clouds in the atmosphere. These droplets also have a considerable sedimentation velocity, so their residence time in the atmosphere is limited, too.

Thus, the small basic droplets and particles, which cause a higher initial sulfate production rate in the parcel would be acidic after a short time under the given pressures of the gases SO_2, H_2O_2 and O_3. The existence of small basic aerosol particles seems to be unrealistic under these conditions. The conclusion is that there are inconsistencies between the chemical composition of the aerosol particles and the pressures of the gases used as input data, which were taken from different measurements. For a future study, the aerosol composition and the pressures of the gases should be taken from a single measurement, in which they are measured simultaneously. In a further extension of the model, the aerosol composition should be brought into equilibrium with the partial pressures of SO_2, NH_3 and HNO_3 in an initial step.

Despite the inconsistencies between the chemical composition of the particles and the pressures of the gases, the results of the present study show under which circumstances the individual oxidants are important. Hydrogen peroxide is the main oxidant in acidic activated cloud droplets and can increase the sulfate mass fractions of the aerosol particles which had acted as condensation nuclei within a short time. In acidic interstitial particles and large cloud droplets, hydrogen peroxide is also an important oxidant. But in these cases, the oxidation catalyzed by an iron–manganese synergism is also important, when the concentrations of the metals are high enough. In basic particles and droplets, ozone is the main oxidant, because the concentrations of iron and manganese ions are small because of the small solubility of the metals. However, the effect of ozone is limited. In basic large droplets and large aerosol particles, the reaction rate depends on the transport of SO_2 and O_3 in the gas phase. Small droplets and particles will be acidic after a short time, if H_2SO_4 is produced. Then, the main oxidant will be no longer ozone, but hydrogen peroxide. There may be one exception: if the pressure of NH_3 is high enough, so that the pH-value of the particle or droplet can be held higher than 4.5 or 5 for a certain time. This point should be investigated by a future version of the model in which the sulfate production over the whole ascent of the parcel is integrated.

7. Summary

The condensational growth of mixed aerosol particles has been described by an adiabatic closed parcel model. The concentrations of ions and catalytic active metals have been calculated in different sized interstitial particles and cloud droplets at a level approximately 370 m above the cloud base. In the activated droplets which have a radius of approximately 5 μm at that level, the ions and the metals have the smallest concentrations of about 10^{-6} to 10^{-4} moles/l for the ions and 10^{-8} to 10^{-7} moles/l for the catalytic active metals. The ions and metals have higher concentrations in the interstitial particles and the large droplets.

Initial sulfate production rates have been calculated based on the concentrations of the ions and the catalytic active metals. In acidic cloud droplets and interstitial particles, sulfate is produced mainly by the reaction of S(IV) with H_2O_2. In droplets with high metal concentrations, the reaction of S(IV) with O_2 catalyzed by a synergism of iron and manganese also makes an important contribution to the sulfate production. In activated droplets, the volume of the electrolyte solution in which the sulfate production occurs, is large compared to the volume of the aerosol particle in the dry state. Even if the droplets are acidic, a sulfuric acid mass equal to the mass of the initial particle is produced in a time comparable to the residence time of a small cumulus. For basic large droplets, the sulfate production rate is limited by gas phase diffusion of SO_2 and O_3. The transport limited rate is smaller by orders of magnitude than the rate calculated under equlibrium conditions. For smaller basic activated droplets and interstitial particles, the sulfate production is not limited by gas-phase diffusion and therefore they should be acidic after a few seconds, under the given pressures of SO_2 and O_3. A consequence of this is that in future study, the input data should be for cases where the gases and the size-dependent chemical composition of the aerosol were measured simultaneously. Further, an initial step to establish equilibrium between the gas pressures and the chemical composition of the particles should be included in the model.

8. Acknowledgements

The author wishes to thank Dr. Ralph Dlugi, Dr. Renate Forkel and Dr. Gottfried Hänel for encouragement and helpful discussions and the unknown reviewers for constructive comments. The study was supported in part by the German Ministry for Science and Technology under contracts 423-4007-0704570 8 and 325-4007-074420 3.

9. Appendix

The condensation model according to Hänel (1987) is used. A special feature of the model is the use of a linearized version of the droplet growth equation. It is presented here in brief. For more complete information, see Hänel (1987).

The linearized droplet growth equation

$$\frac{dr^2}{dt} = -2D_b\delta_{rb}r^2 + 2D_b\delta_f(t-t_b) + 2D_b(f_b - f_{rb} + \delta_{rb}r_b^2), \tag{2.1}$$
$$\tag{A.1}$$

can be solved analytically with the solutions:

$$r^2 = r_b^2 + 2D_b(f_b - f_{rb})(t-t_b) + D_b\delta_f(t-t_b)^2 \quad \text{for } \delta_{rb} = 0, \tag{A.2}$$

$$r^2 = r_b^2 + \left\{\delta_f(t-t_b) + \left[f_b - f_{rb} - \frac{\delta_f}{2D_b\delta_{rb}}\right] \times \left[1 - \exp(-2D_b\delta_{rb}(t-t_b))\right]\right\}\delta_{rb}^{-1}, \quad \text{for } \delta_{rb} \neq 0. \tag{A.3}$$

Here the subscript b denotes the value at the beginning of the time step. f is the relative humidity of the environment, f_r the relative humidity immediately above the surface of the droplet. r is the radius of the droplet, D the parameter for water vapor diffusion in air corrected for the heat transfer between the droplet and the environment, and δ_f the change of the environmental relative humidity with time:

$$\delta_f = \frac{df}{dt}. \tag{A.4}$$

δ_r is defined as

$$\delta_r = \frac{df_r}{dr^2}. \tag{A.5}$$

From eq. (A.3), it can be seen that for a particle for which an equilibrium radius exists ($\delta_r < 0$), a thermodynamic relaxation time can be defined as

$$\tau_b = (2D_b\delta_{rb})^{-1}. \tag{A.6}$$

Hänel (1987) compared this new method with the conventional Runge–Kutta-Method and found deviations smaller than 1% in the radius for particles with dry volume equivalent radii larger than 1 μm. Larger deviations up to 3.3% occur only for smaller particles and a very small change of the ambient relative humidity δ_f.

REFERENCES

Blyth, A. M. and Latham, J. 1985. An airborne study of vertical structure and microphysical variability within a small cumulus. *Quart. J. R. Met. Soc. 111*, 773–792.

Brosset, C. 1976. Air-borne particles: black and white episodes. *AMBIO 5*, 157–163.

Davis, B. L. 1984. X-ray diffraction analysis and source apportionment of Denver aerosol. *Atmos. Environ. 18*, 2197–2208.

Davis, B. L. and Maughan, A. D. 1984. Observation of heavy metal compounds in suspended particulate matter at east Helena, Montana. *JAPCA 34*, 1198–1202.

Deer, W. A., Howie, R. A. and Zussmann, J. 1963. *Rock forming minerals.* New York: John Wiley and Sons.

Diem, M. 1948. Measurements of the size of cloud elements (in German). *Meteorologische Rundschau 1*, 261–273.

Fitzgerald, J. W., Hoppel, W. A. and Vietti, V. A. 1982. The size and scattering coefficient of urban aerosol particles at Washington, DC as a function of relative humidity. *J. Atmos. Sci. 39*, 1838–1852.

Handbook of Chemistry and Physics. 66th edition 1985. Boca Raton Florida: CRC Press Inc.

Hänel, G. 1976. The properties of atmospheric aerosol particles as functions of the relative humidity at thermodynamic equilibrium with the surrounding moist air. *Advances in Geophysics 19*, 73–188.

Hänel, G. 1987. The role of aerosol properties during the condensational stage of cloud: Reinvestigation of numerics and microphysics. *Contrib. Atmos. Phys. 60*, 321–339.

Hänel, G. and Lehmann, M. 1981. Equilibrium size of aerosol particles and relative humidity: new experimental data from various aerosol types and their treatment for cloud physics application. *Contrib. Atmos. Phys. 54*, 57–71.

Harrison, R. M. and Pio, C. A. 1981. Apparatus for simultaneous size-differentiated sampling of optical and suboptical aerosols: applications to analysis of nitrates and sulfates. *JAPCA 31*, 784–787.

Heikes, B. G., Gregory, L. R., Walega, J. G. and Lazrus, A. L. 1987. H_2O_2, O_3 and SO_2 measurements in the lower troposphere over the eastern United States during fall. *J. Geophys. Res. 92*, No. D1, 915–931.

Hennes, E.-Ch. 1983. Development of a chemical equilibrium model for water describing complexes and experimental testing for water of the river Rhine (in German). *Report of Kernforschungszentrum Karlsruhe, KfK 3599.*

Hoffmann, M. R. and Calvert, J. G. 1985. *Chemical transformation modules for eulerian acid deposition models. Volume II: The aqueous-phase chemistry.* Project Report, Acid Deposition Modeling Project, National Center for Atmospheric Research, P.O. Box 3000, Boulder, Colorado 80307.

Höfken, K. D., Georgii, H. W. and Gravenhorst, G. 1981. Investigation of deposition of atmospheric trace constituents in beech and spruce forest (in German). *Report of the Institute for Meteorology and Geophysics of the University Frankfurt/Main No.46.*

Hoppel, W. A. 1979. Measurement of the size distribution and CCN supersaturation spectrum of submicron aerosols over the ocean. *J. Atmos. Sci. 36*, 2006–2015.

Hough, A. M. 1987. A computer modeling study of the chemistry occurring during cloud formation over hills. *Atmos. Environ. 21*, 1073–1095.

Hwang, H. and Dasgupta, P. K. 1983. Thermodynamics of the hydrogen peroxide–water system. *Environ. Sci. Technol. 19*, 255–258.

Ibusuki, T. and Takeuchi, K. 1987. Sulfur dioxide oxidation by oxygen catalyzed by mixtures of manganese(II) and iron(III) in aqueous solutions at environmental reaction conditions. *Atmos. Environment 21*, 1555–1560.

Jensen, J. B. and Charleson, R. J. 1984. On the efficiency of nucleation scavenging. *Tellus 36B*, 367–375.

Lee, I.-Y. 1986. Numerical simulation of chemical and physical properties of cumulus clouds. *Atmos. Environ. 20*, 767–771.

Lindberg, S. E. and Harriss, R. C. 1983. Water and acid soluble trace metals in atmospheric particles. *J. Geophys. Res. 88, No. C9*, 5091–5100.

Maahs, H. G. 1983. Kinetics and mechanisms of the oxidation of S(IV) by ozone in aqueous solution with particular reference to SO_2 conversion in nonurban clouds. *J. Geophys. Res. 88*, 10721–10732.

Martin, L. R. 1984. Kinetic studies of sulfite oxidation in aqueous solution. In *SO_2, NO and NO_2 oxidation mechanisms: atmospheric considerations* (ed. J. G. Calvert). Boston: Butterworth Publishers, 1984, 63–100.

Milford, J. B. and Davidson, C. I. 1985. The sizes of particulate trace elements in the atmosphere—a review. *JAPCA 35*, 1249–1260.

Mordy, W. 1959. Computation of the growth by condensation of a population of cloud droplets. *Tellus 11*, 16–44.

Pruppacher, H. R. and Klett, J. D. 1978. *Microphysics of clouds and precipitation.* Dordrecht, Holland: D. Reidel Publishing Company.

Reible, D. D., Ouimette, J. R. and Shair, F. H. 1982. Atmospheric transport of visibility degrading pollutants into the California Mojave desert. *Atmos. Enviorn. 16*, 599–613.

Richter, F.-W. and Wätjen, U. 1980. Trace metal composition of settling dust and ambient aerosol close to a highway. Gesellschaft für Aerosolforchung. *Proceedings 8. Conference, 22–24 October, 1980, Schmallenberg, Germany F.R.*, 84–89.

Schumann, T., Zinder, B. and Waldvogel, A. 1986. Measurements of aerosol and hydrometeor concen-

trations and their chemical composition during winter precipitation along a mountain slope. *AEROSOLS: Formation and Reactivity; 2nd Int. aerosol Conf. Berlin.* Oxford: Pergamon Journal Ltd., 67–70.

Schwartz, S. E. and Freiberg, J. E. 1981. Mass-transport limitations to the rate of reaction of gases in liquid droplets: application to oxidation of SO_2 in aqueous solutions. *Atmos. Environ. 15*, 1129–1144.

Sloane, C. S. 1984. Optical properties of aerosols of mixed composition. *Atmos. Environ. 18*, 871–878.

Stelson, A. W. and Seinfeld, J. H. 1981. Chemical mass accounting of urban aerosol. *Atmos. Environ. 15*, 671–679.

Stumm, W., Sigg, L. and Schnoor, J. L. 1987. Aquatic chemistry of acid deposition. *Environ. Sci. Technol. 21*, 8–13.

Thudium, J. 1978. Water uptake and equilibrium sizes of aerosol particles at high relative humidities: their dependence on the composition of the water-soluble material. *Pageoph 116*, 130–148.

Tremblay, A. and Leighton, H. 1986. A three-dimensional cloud chemistry model. *J. of Climate and Appl. Meteor. 25*, 652–671.

Walcek, Ch. H. and Taylor, G. R. 1986. A theoretical method for computing vertical distributions of acidity and sulfate production within cumulus clouds. *J. Atmos. Sci. 43*, 339–355.